Journal of ELECTRONIC MATERIALS, Vol. 39, No. 8, 2010
DOI: 10.1007/s11664-010-1236-y

Carboxylate-Passivated Silver Nanoparticles and Their Application to Sintered Interconnection: A Replacement for High Temperature Lead-Rich Solders

HIROSHI OGURA,[1] MINORU MARUYAMA,[1,2,7] RYO MATSUBAYASHI,[3] TETSUYA OGAWA,[4] SHIGEYOSHI NAKAMURA,[5] TERUO KOMATSU,[1,2] HIROSHI NAGASAWA,[2] AKIO ICHIMURA,[6] and SEIJI ISODA[4]

1.—Applied Nanoparticle Laboratory, Incubator, Osaka City University, Osaka 558-8585, Japan. 2.—Department of Physics, Osaka City University, Osaka 558-8585, Japan. 3.—Shindengen Electric Manufacturing Co., Ltd., Hanno, Saitama 357-8585, Japan. 4.—Institute for Chemical Research, Kyoto University, Uji, Kyoto 611-0011, Japan. 5.—Bruker AXS K. K., Yokohama 221-0022, Japan. 6.—Department of Chemistry, Osaka City University, Osaka 558-8585, Japan. 7.—e-mail: maruyam@sci.osaka-cu.ac.jp

Lead-free silver nanoparticle pastes have been tested as a replacement for high temperature lead-rich solders used in electronic manufacturing. The pastes contain a small amount of solvent, and primarily consist of submicron-silver powder and passivated silver nanoparticles. The nanoparticles were synthesized from Ag_2CO_3 and a long-chain alcohol by a method that produced a passivating layer consisting almost exclusively of the carboxylate of the reactant alcohol. The pastes were used to connect a silicon diode chip to copper bases without applied pressure when sintered at 350°C under nitrogen. Diode packages made with sintered silver interconnects had electrical and thermal properties equal to those with lead-soldered interconnects, even after 3000 thermal cycles between −55°C and +150°C. The mechanical strength was half that of lead-rich solder joints, but still strong enough for practical use.

Key words: Carboxylate-passivated silver nanoparticles, low-temperature sintering, sintered interconnection, high temperature lead-free solder, thermal cycling test

INTRODUCTION

Due to lead's toxicity, there have been numerous attempts for replacing lead-based alloy solders with lead-free alternatives. The primary eutectic Sn-Pb alloys (melting point 183°C) have already been replaced with the Sn-Ag-Cu (SAC) alloys.[1] However, despite candidates such as Au-Sn and Zn-Sn alloys,[2] there are no suitable lead-free high temperature solders (i.e., melting point >250°C). The high temperature solders containing 90-95 wt.% Pb are still widely used in various applications. Due to the lack of suitable non-lead alternatives, the high temperature solders are exempted from the Restriction of Hazardous Substances (RoHS) Directive (exemption 7a in Annex to RoHS Directive). This exemption is periodically reviewed and revised every few years. If the high temperature solders are phased out, a comparable non-lead replacement will be needed.

Other lead-free, high temperature alternatives include conductive adhesives.[2,3] All conductive adhesives consist of epoxy resin and metal fillers. The resin makes metallic connections between the fillers, and between the fillers and a base. The resin joints provide stable interconnections, making conductive adhesives an attractive lead-free solder replacement. Nevertheless, conductive adhesives have several drawbacks such as a susceptibility to conductivity fatigue caused by oxidation and humidification at the interface, poor impact strength, poor thermal shock resilience, and low overall conductivity due to the nonconductive resin. Although efforts are being made to overcome the problems,[3]

(Received November 13, 2009; accepted April 7, 2010; published online May 1, 2010)

much more progress is necessary before conductive adhesives are ready for implementation.

Silver nanoparticles provide another promising lead-free, high temperature alternative.[4–7] Due to the size effect, silver nanoparticles have significantly lower melting temperatures than the 960°C value for bulk silver. For example, a molecular dynamics simulation shows that 2.4 nm silver nanoparticles melt at about 350°C, and the nanoparticle surface layer melts at even lower temperature.[8] Because of capillary pressure between contacting nanoparticles, the surface-melted nanoparticles sinter easily, even without external pressure, eventually forming sintered metallic silver with a bulk melting temperature of 960°C. Moreover, the sintered silver adheres strongly to a copper base.[7] These reasons make silver nanoparticles a leading candidate for the lead-free high temperature solder alternative.

The outer surface of the silver nanoparticles was passivated to prevent spontaneous aggregation and coalescence. Passivation was done in two ways. One way was to synthesize the nanoparticles from silver carbonate (Ag_2CO_3) in 1-dodecanol, isolating them by precipitation and filtration. The other way used 1-decanol instead of 1-dodecanol. Much of the passivating layer was removed by heating the particles, allowing the bare nanoparticles to sinter and form highly conductive, durable, and strong interconnections.

In this paper, we characterize the silver nanoparticles synthesized from Ag_2CO_3 and 1-dodecanol. The samples were refined by suspending the nanoparticles in hexane. Nanoparticles synthesized from 1-decanol could not be suspended in hexane and, therefore, were not used for chemical characterization. The nanoparticles were used to form sintered interconnections in diode packages, and those packages' thermal and electrical resistances were measured during and after thermal cycling. For this study, the diode packages were thermally cycled 3000 times as continued from the 1800-cycle measurements presented in our previous work.[7] The shear strength and fracture surfaces of sintered joints also were examined. The results show that the silver nanoparticles are viable lead-free alternative to lead-rich high temperature solders.

EXPERIMENTAL

Chemical Characterization and Thermal Behavior

Synthesis of Silver Nanoparticles

The silver nanoparticles were made by heating silver carbonate (Ag_2CO_3, 99.9% purity, Inuisho Precious Metals, 20 g) in either 1-dodecanol ($CH_3(CH_2)_{11}OH$, 97%+ purity, Kishida Chemical, 200 g) or 1-decanol ($CH_3(CH_2)_9OH$, 97%+ purity, Kishida Chemical, 200 g) at 140–180°C for 5-10 min, as reported previously.[7] The silver nanoparticles were precipitated from the reaction mixture by adding ethanol. For the subsequent chemical characterization, the nanoparticles synthesized from 1-dodecanol were refined by recovering the portion suspendable in hexane. The yield of the refined nanoparticles was 5 g. The nanoparticles synthesized from 1-decanol could not be suspended in hexane, and therefore were not refined. Although these nanoparticles could not be used for the chemical characterization, the sintered joints made from them showed slightly better electrical properties than the joints made from the 1-dodecanol-derived nanoparticles.

TEM of Silver Nanoparticles

Transmission electron microscopy (TEM) was done using a JEOL JEM-2000FX transmission electron microscope, operating at 200 kV. The silver nanoparticles were suspended in hexane and applied on a carbon-film coated copper grid before observation.

GC-MS

A sublimation apparatus was used to prepare the samples. The nanoparticles (100–200 mg) were heated at 230°C under reduced pressure to gasify the organic layer, which in turn was condensed onto the cold finger filled with liquid nitrogen. The condensed organic layer was dissolved in hexane. A gas chromatograph /mass spectrometer (Varian Saturn 4D, ion trap mass analyzer with electron ionization(+)) was used for the analysis. The column used for the chromatography was of the DB-5 capillary type.

LDI-TOF

The laser desorption ionization/time-of-flight (LDI-TOF) mass spectra were taken using a Shimadzu AXIMA-CFR spectrometer equipped with an N_2 laser (337 nm wavelength). The silver nanoparticles were suspended in hexane and placed on a sample plate for measurement. Both cation and anion detection modes were used.

TG-DSC-IR

The thermo-gravimetry /differential scanning calorimetry/infra-red spectroscopy (TG-DSC-IR) measurements were performed on a Netszch STA449C Jupiter TG-DSC connected to a Bruker Optics Tensor 27 FT-IR. The sample mass used was 2–5 mg. The sample temperature was raised at the rate of 10°C/min from 40°C to 500°C, under the flow of N_2 or air at the rate of 40 mL/min. The IR spectra were measured in the gas phase.

Formation and Testing of Sintered Joints

Silver Nanoparticle Paste

The same pastes as those in the previous paper[7] were used. For the preparation, 40 g of the unrefined silver nanoparticles synthesized in

1-dodecanol and 60 g of silver powder (diameter 0.3 μm) were mixed into 10 g of isobornyl cyclohexanol (IBCH). The final silver content was 87 wt.%. A similar paste was made by mixing 15 g of the unrefined silver nanoparticles synthesized in 1-decanol and 80 g of the silver powder with 10 g of IBCH (final silver content 89 wt.%).

Preparation and Electrical Testing of Diode Packages

The diode packages for testing the electrical properties of joints (sintered silver or high temperature Pb-5Sn solder) were assembled as previously described.[7] The diode chip was gold-plated, and sintered joints connecting gold to copper bases were formed at 350°C in N_2 or at 300°C in air. Epoxy resin was added around the sintered joints for protection. Thirty packages were prepared for each paste-atmosphere combination, and tested by measuring the forward voltage. One package from each paste-atmosphere combination was sliced perpendicularly to the sintered silver/copper base interface. The cross-sectional surface was filed to trim the debris, and then observed by scanning electron microscopy (SEM, JEOL JSM-7600FA). The remaining packages were subjected to repeated electrical testing and thermal cycling. The electrical resistance was obtained from the forward voltage V_F measured at a constant current. The thermal resistance was from the difference ΔV_F in forward voltage between before and after Joule heating of the diode. Thermal cycling was done between −55°C and +150°C.

Shear Strength and Fracture Surface

The paste was applied to an oxygen-free copper base (11 mm × 8 mm × 1 mm), then the applied paste was covered with an oxygen-free copper disk (5 mm diameter, 2 mm thickness). A pressure of 1 MPa was applied for 10 s. The assembly was then sintered with either an increasing–decreasing temperature profile of 18 min with the minima at ambient temperature and the maximum at 350°C (in N_2), or an increasing–decreasing profile with a plateau at 300°C for 20 min (in air). During the heating, either 1 MPa pressure or no pressure was applied. Similar joints were made using Pb-5Sn alloy solder paste in N_2. For the fracture strength measurements, the joints were placed on a bond tester (DAGE Series 4000P, equipped with a DS100 load cell) and the disk was pushed parallel to the base with a shear speed of 100 μm/s until the joint broke. For each type of joint, ten samples were prepared and tested. The fracture surfaces were observed by SEM.

RESULTS AND DISCUSSION

TEM of the Silver Nanoparticles

Figure 1 shows close-packed assemblies of silver nanoparticles with a 3–6 nm diameter. TEM observation shows metallic silver core images but does not show images for the organic layers coating the silver surface. These organic passivating layers prevent the direct contact between the silver surfaces and, therefore, prevent coalescence. There are also larger nanoparticles (10–100 nm in diameter) that constitute about 70 wt.% of the original unrefined sample. The larger nanoparticles are not observed in Fig. 1 because of their poor dispersion in hexane.

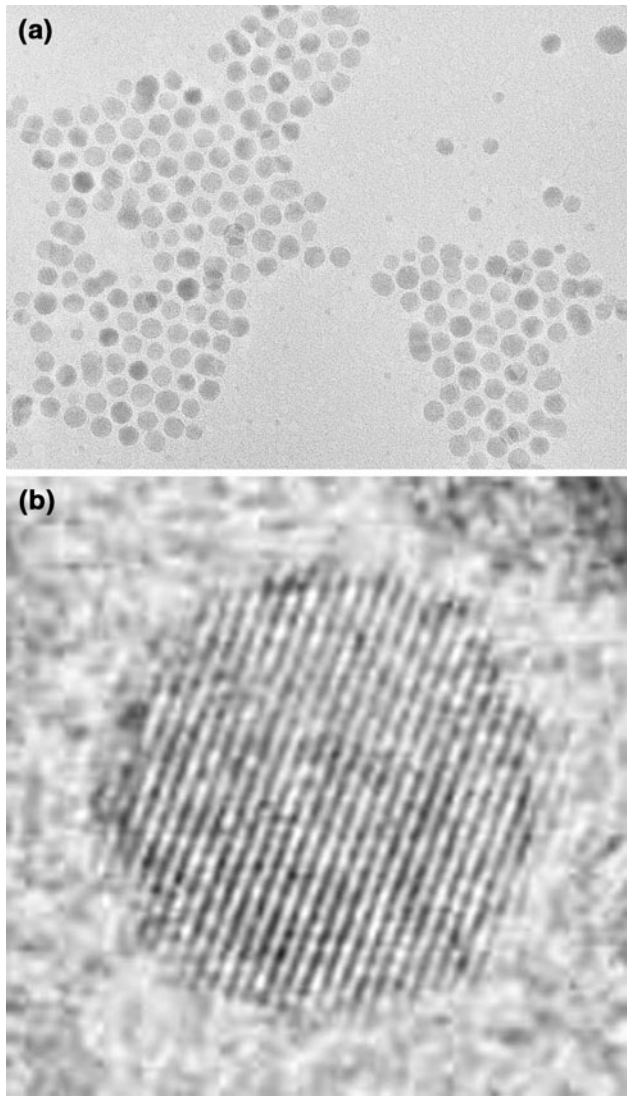

Fig. 1. TEM images of (a) the silver nanoparticles synthesized from Ag_2CO_3 and 1-dodecanol, and (b) one of the nanoparticles, enlarged to show the {111} lattice planes with 0.23-nm spacing.

GC-MS and LDI-TOF of the Passivating Organic Layer

Figure 2 shows gas chromatograms for the passivating organic layer of the silver nanoparticles synthesized in 1-dodecanol, and chromatographic standard compounds of 1-dodecanol, 1-dodecanoic acid, and 1-undecanoic acid. The major GC trace

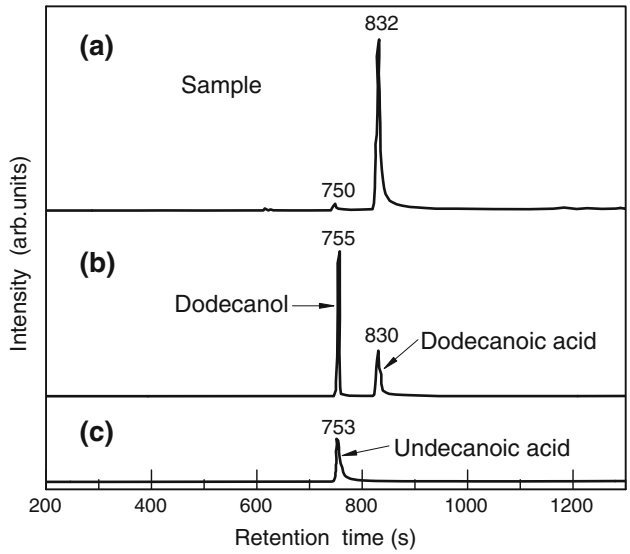

Fig. 2. Gas chromatograms of (a) the organic layer of the silver nanoparticles synthesized in 1-dodecanol, (b) a mixture of the 1-dodecanol and 1-dodecanoic acid standards, and (c) the 1-undecanoic acid standard.

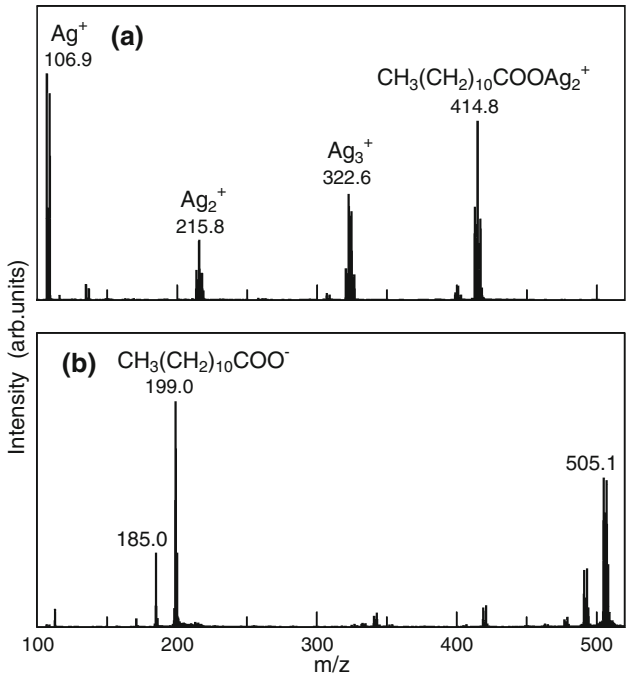

Fig. 3. LDI-TOF mass spectra of the silver nanoparticles synthesized in 1-dodecanol. (a) Positive detection mode. (b) Negative detection mode. The quantity *m/z* is molecular mass per charge of the detected ion, the charge unit being the elementary charge.

peak at 832-s retention time (Fig. 2a) coincides with that for the 1-dodecanoic acid standard (Fig. 2b), and indicates that the organic layer around the silver nanoparticles consists overwhelmingly of 1-dodecanoate. The minor peak with the retention time of 750 s, which at first appears to be coincident with that of the dodecanol standard, is actually caused by 1-undecanoic acid (Fig. 2c, as confirmed by the MS fragmentation pattern, not shown). Figure 3 is laser desorption ionization/time of flight (LDI-TOF) mass spectra of the silver nanoparticles. The m/z = 414.8 peak in the positive detection mode spectrum (Fig. 3a) is consistent with a dodecanoate anion bound to two silver cations, and indicates that dodecanoate is bonded to silver atoms in the silver nanoparticles. The major m/z = 199.0 peak in the negative detection mode spectrum (Fig. 3b) indicates the presence of dodecanoate anions. The m/z = 505.1 peak is consistent with bis(dodecanoato)silver(I) anion. The minor m/z = 185.0 peak is consistent with the undecanoate anion. These peaks are the only ones that are detected consistently in the negative detection mode. The other minor peaks are detected at varying intensity from measurement to measurement and, therefore, are likely caused by residual impurities inside the sample chamber of the spectrometer.

We conclude that 1-dodecanol was converted to 1-dodecanoate during the reaction with silver carbonate and/or silver nanoparticles. Although the nanoparticles synthesized from 1-decanol were not subjected to a similar chemical characterization, they too are expected to be passivated with the corresponding carboxylate of 1-decanol. Such conversion has many precedents.[9,10] Silver is known to serve as a catalyst for the oxidation of primary alcohols to their corresponding aldehydes. Such aldehydes are easily oxidized further to the corresponding carboxylic acids under the present synthetic condition. Furthermore, a carboxylic acid has much stronger affinity to silver than the corresponding alcohol because of the former's chelating ability and, therefore, the carboxylate ligation to silver nanoparticles is more probable than the alkoxide ligation that was postulated in the previous work.[7] As for the observed 1-undecanoic acid, it is possibly a decarboxylation product of 1-dodecanoate. Such decarboxylation is known to occur in the presence of transient Ag^{II} cations.[11,12]

TG-DSC-IR of the Passivating Carboxylate Layer in N_2

The IR spectra in the TG-DSC-IR measurements were used for identifying the vibrational signals from the alkyl C–H bonds (C–H, 3100–2900 cm^{-1}) and the C=O bonds from CO_2 (O=C=O, 2400–2300 cm^{-1}). These signals were integrated to obtain the relative emission of the hydrogenated organics and CO_2, respectively.

The TG-DSC-IR data taken in N_2 are shown in Fig. 4. The TG plot in Fig. 4a indicates that a weight loss (13%) occurs from 200°C to 280°C. The DSC plot in the same figure indicates that the weight loss from 200°C to 260°C is slightly endothermic, and the loss from 260°C to 280°C is highly exothermic with the DSC peak at 267°C. The integrated IR trace of the C–H signal in Fig. 4b

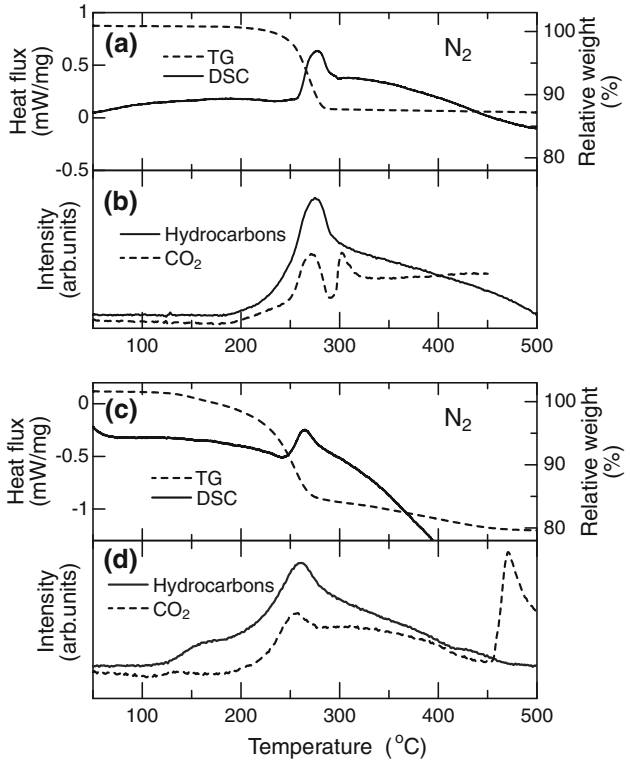

Fig. 4. Thermal behavior of the carboxylate layer in N_2. (a) TG and DSC plots and (b) IR traces of the nanoparticles synthesized from Ag_2CO_3 and 1-dodecanol. (c) TG and DSC plots and (d) IR traces of the nanoparticles synthesized by pyrolysis of silver dodecanoate.

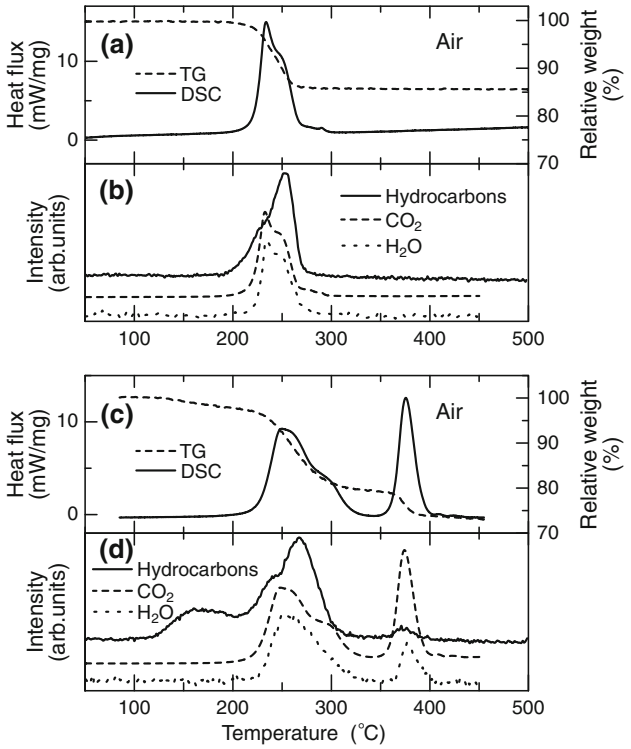

Fig. 5. Thermal behavior of the carboxylate layer in air. (a) TG and DSC plots and (b) IR traces of the nanoparticles synthesized from Ag_2CO_3 and 1-dodecanol. (c) TG and DSC plots and (d) IR traces of the nanoparticles synthesized by pyrolysis of silver dodecanoate.

indicates that the organic component of the outer layer begins volatilizing at 190°C, and the volatilization continues toward 500°C. The trace has a peak at 267°C, coincident with the exothermic DSC peak in Fig. 4a. The integrated IR trace of the O=C=O signal in Fig. 4b indicates that the CO_2 emission begins at 190°C and maximizes at 267°C, which is coincident with the DSC and the C–H trace peaks. The near-identical shapes of the O=C=O and the C–H traces up to 290°C indicates that the CO_2 emission up to that temperature is caused by decarboxylation of the ligated dodecanoate. The O=C=O trace shows another peak at 303°C, which has no counterpart in the TG, the DSC, or the C–H trace plot. A possible explanation is that a trace amount of Ag_2CO_3 (a starting material) remains among the nanoparticles, and this Ag_2CO_3 decomposes at 303°C.

Dodecanoate-passivated silver nanoparticles synthesized by a different method were also characterized by TG-DSC-IR. These nanoparticles, previously reported,[13] were synthesized by pyrolysis of silver dodecanoate at 250°C in N_2. The GC-MS and LDI-TOF data of these nanoparticles (not shown) indicate that their passivating organic layer is identical to that of the nanoparticles synthesized in 1-dodecanol. The IR traces measured in N_2 (Fig. 4d) show a large O=C=O peak at 470°C. There is no corresponding TG or DSC peak in Fig. 4c.

TG-DSC-IR of the Passivating Caboxylate Layer in Air

The TG-DSC-IR data taken in air, as shown in Fig. 5, are characterized by a strong exothermic DSC peak (Fig. 5a, c) that is coincident with large O=C=O and H–O–H peaks (Fig. 5b,d) characteristic of aerobic oxidation of the organic passivating layer. The TG plot (Fig. 5a) and the C–H trace (Fig. 5b) of the nanoparticles synthesized from 1-dodecanol show very little decrease after the aerobic oxidation peaks, indicating that the organic layer became almost completely gasified after the oxidation.

The TG-DSC data from the nanoparticles synthesized by silver dodecanoate pyrolysis (Fig. 5c) shows a large exothermic DSC peak and a corresponding TG drop at 380°C. The corresponding IR trace (Fig. 5d) shows a large O=C=O peak at the corresponding temperature. These peaks are caused by the pyrolysis byproduct which has low-volatility and is most likely to be a free-radical polymerization product of the dodecanoate anion. The TG-DSC-IR samples of the nanoparticles synthesized by pyrolysis remained grey after the measurement, indicating that a significant amount of nanoparticles were incompletely reacted. Such silver nanoparticles are not expected to form suitable sintered joints.

The TG-DTA-IR measurements from the passivated silver nanoparticles indicate that the passivating layer gasifies more completely in air than N_2.

Therefore, it was expected that a sintered silver mass with better conductivity and a higher structural strength could be obtained by carrying out the sintering in air rather than N_2. Accordingly, we decided to examine electrical and mechanical properties for joints sintered both in air and N_2. On the other hand, sintering in air inevitably causes the formation of a copper oxide layer whenever a copper base is used. The detrimental effects of copper oxide layer, such as decreased electrical conductivity, weaker silver-copper interface, and mismatch in the expansion coefficients, are well known.

Silver Nanoparticle Pastes

The pastes were made by mixing unrefined silver nanoparticles with IBCH solvent and silver filler powder (diameter 300 nm). Silver powder was added to increase the silver weight percentage, thereby decreasing the relative amount of organic material that converts into void-causing gas upon sintering. The unrefined nanoparticles (3–100 nm), together with the filler powder, also widened the size distribution of silver particles, thus making the final structure denser and stronger (analogous to the strengthening of concrete through gradation of aggregates). The paste made from the nanoparticles synthesized from 1-decanol (hereby abbreviated as "C10Ag" paste) showed slightly better electrical properties than those synthesized from 1-dodecanol (hereby abbreviated as "C12Ag" paste) when sintered as indicated below.

SEM of Silver/Copper Interface

Figure 6 shows cross-sectional SEM images for the silver-copper interface formed in a diode package when the gold-plated diode chip was connected to copper bases with sintered silver. For the diode package sintered in N_2 (Fig. 6a), the interface between the sintered silver and the copper base is unbroken and smooth. On the other hand, for the package sintered in air (Fig. 6b), a copper oxide (Cu_xO, x = 1 or 2) layer is present between them. Copper (I or II) oxide is an electrical and thermal insulator with a dissimilar thermal expansion coefficient compared to either copper or silver metal, and therefore is expected to have a detrimental effect on the interconnector performance. The detrimental effect, as determined experimentally, will be explained below.

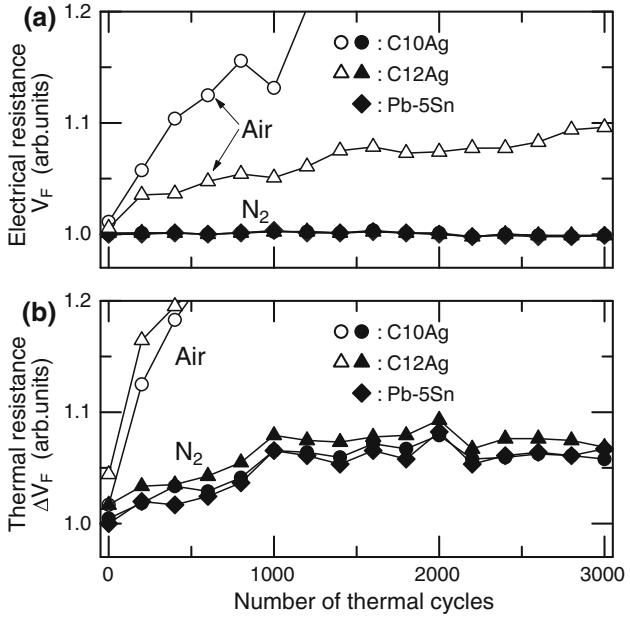

Fig. 7. Graphs of (a) electrical resistances V_F and (b) thermal resistances ΔV_F of diode packages made from each paste. Circles: C10Ag paste. Triangles: C12Ag paste. Open: sintered in air. Solid: sintered in N_2. Diamonds: high temperature Pb-5Sn solder paste.

Thermal Cycling and Electrical Measurements

Figure 7 shows the electrical (V_F) and thermal (ΔV_F) resistances for the diode packages after 3000

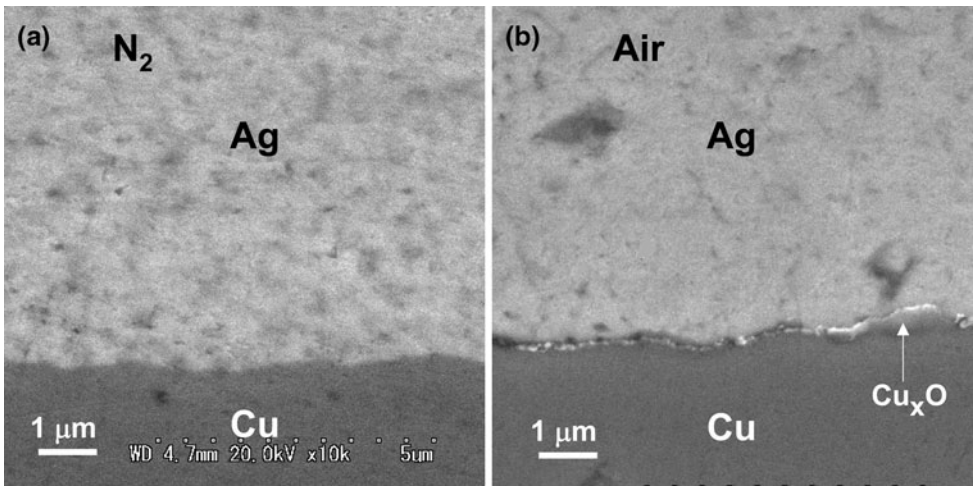

Fig. 6. SEM images of a sintered silver/copper base interface made using the C12Ag paste (a) in N_2, and (b) in air. In (b), a layer of copper oxide (Cu_xO, x = 1 or 2) is visible.

thermal cycles (as continued from the 1800-cycle measurements presented in the previous paper[7]). The values for both V_F and ΔV_F are normalized with respect to the V_F and ΔV_F values at zero thermal cycle for the joint made with the Pb-5Sn solder paste.

Figure 7a shows plots for V_F. For all the diode packages sintered in N_2, there is no observable change from the initial value (1.00) even after 3000 thermal cycles. On the other hand, for the diode packages sintered in air, the V_F values of the C12Ag paste increase steadily to 1.1 after 3000 cycles. As for the C10Ag paste, the increase is even steeper, up to V_F = 1.3 (off-scale in Fig. 7a) after 3000 cycles.

Figure 7b shows plots for ΔV_F. For the diode packages sintered in N_2, the ΔV_F values stabilize at 1.05 after 1000 cycles, and remains virtually unchanged up to 3000 cycles. Just as with the V_F values, very little difference from those for the lead-rich solder is observed. The values for the C10Ag paste are slightly lower than those for the C12Ag paste. The ΔV_F values for the diode packages sintered in air increase rapidly for both C10Ag and C12 Ag pastes, until they reach 1.4 and 1.3, respectively (off-scale in Fig. 7b) after 3000 cycles.

The initial V_F and ΔV_F values indicate that neither the N_2- nor the air-sintered joints offer a significant advantage before thermal cycling. These values suggest that any advantage offered by the complete volatilization of the organic layer in air is offset by the disadvantage caused by the copper oxide layer. The thermal cycling data show that the detrimental effect of sintering in air far outweighs the advantages. The rapid increase in both the V_F and the ΔV_F values during thermal cycling is very likely caused by the mismatched thermal expansion/contraction rates between the copper oxide and metal layers and the subsequent oxide layer delamination.

Shear Strength and Fracture Surface

Table I shows shear strengths for sintered silver joints. Because of the slightly lower and consequently better ΔV_F values, the C10Ag paste (rather than the C12Ag paste) was used for the shear strength and fracture surface experiments.

There were no significant shear strength differences between the joints sintered in N_2 (12 MPa) and the ones sintered in air (11 MPa). This suggests that any advantage from the better volatilization of the passivating layer in air was offset by copper oxide formation at the silver-copper interface. The shear strength increases 2- to 3-fold when 1 MPa pressure is applied during sintering, but such pressure application is not favorable to automated manufacturing process. Although the joints sintered without pressure application are weaker than those sintered at 1 MPa pressure, their strength is sufficient for most practical applications where the joint is protected and strengthened by an encapsulating epoxy resin.

Figure 8 is SEM images of joint fracture surfaces. Joints formed with no pressure applied, whether sintered in N_2 (Fig. 8) or air (not shown), give rise to irregular fracture surfaces with raised regions ("lands") and lowered regions ("seas"). This suggests that structural strength throughout the joints is uneven with weak spots randomly scattered throughout the joint. High resolution SEM images (Fig. 8c–f) show that fractures occur at the copper-silver interface (Fig. 8c, d) and inside the sintered silver mass (Fig. 8e, f). On the other hand, joints formed with 1 MPa applied pressure (not shown),

Table I. Shear strength of the sintered joints made from C10Ag paste

Pressure Applied During Sintering (MPa)	Sintering Atmosphere	Shear Strength (MPa)
0	N_2	12
0	Air	11
1	N_2	32
1	Air	26
0[a]	N_2	24

[a]High temperature Pb-5Sn solder paste.

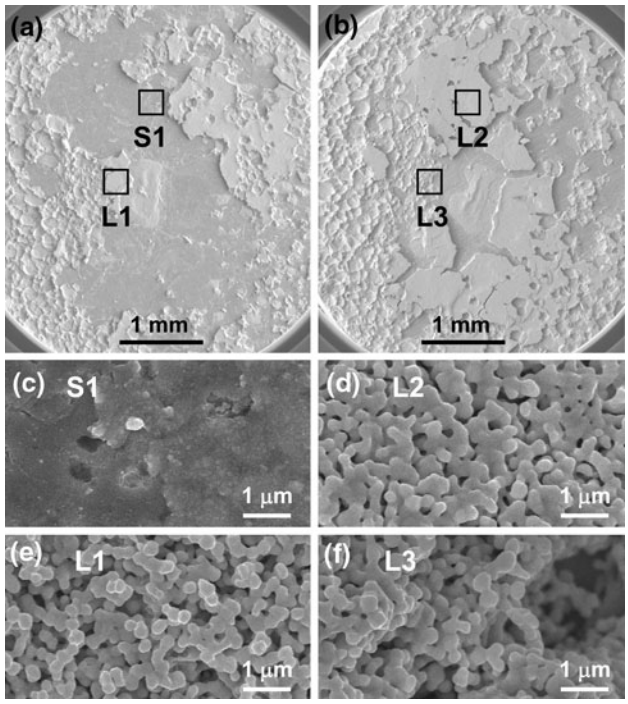

Fig. 8. SEM images of the fracture surface of a joint made from the C10Ag paste, sintered in N_2, no pressure applied during sintering. (a) Lower surface and (b) upper surface reversed left and right. (c) S1 region (copper base) and (d) L2 region (sintered silver), fractured at the copper-silver interface. (e) L1 region (sintered silver) and (f) L3 region (sintered silver), fractured inside the sintered silver mass.

sintered in either air or N_2, fracture only inside the sintered silver mass (even though some river-like voids can be seen). These fracture surfaces suggest that the joints are homogeneous, with a uniform structural strength throughout the sintered mass, and stronger bonding at the interface. This structural homogeneity (i.e. without "weak spots") logically leads to stronger shear strength. No apparent difference could be seen between the fracture surfaces of the N_2-sintered and the air-sintered joints regardless of the sintering pressure.

CONCLUSION

We found the passivating layer for the nanoparticles made from Ag_2CO_3 and primary alcohol to consist of the carboxylate corresponding to the alcohol. Moreover, the passivating layer contained fewer nonvolatile impurities than was the case for the nanoparticles synthesized by pyrolysis of silver carboxylate. Therefore, the alcohol-derived nanoparticles were better suited for sintering. When the passivating layer gasifies during heating, the bare nanoparticles are sintered with the silver filler particles into a strong, highly conductive silver mass. This sintered mass, when formed on a copper base in N_2, adhered to the base and became an excellent electrical and thermal interconnect. Moreover, this sintered joint retained its electrical and thermal resistances even after 3000 thermal cycles between −55 and +150°C.

The electrical and thermal properties of the joints sintered in air were comparable to those sintered in N_2 before thermal cycling. However, when the joints were subjected to thermal cycling, both properties deteriorated steeply for the joints sintered in air, while those for the joints sintered in N_2 remained virtually unchanged. The strength of the joints formed by sintering at ambient pressure was half that of lead-rich solder joints, but they would be sufficiently strong for practical use given the extra protection that is added by the epoxy resin in the packaging. The silver nanoparticle paste can easily fit into current automated manufacturing lines not provided with a means for soldering under pressurization. This easy automation, together with the endurance under thermal cycling, makes our silver nanoparticle paste a viable replacement for the high temperature lead-rich solder.

ACKNOWLEDGEMENTS

This work was supported by KAKENHI 19540343. Part of this work was conducted in Kyoto-Advanced Nanotechnology Network, supported by "Nanotechnology Network" of the MEXT, Japan.

REFERENCES

1. I.E. Anderson, *J. Mater. Sci.-Mater. Electron.* 18, 55 (2007).
2. K. Suganuma, S.J. Kim, and K.S. Kim, *JOM* 61, 64 (2009).
3. Y. Li and C.P. Wong, *Mater. Sci. Eng. R* 51, 1 (2006).
4. K.S. Moon, H. Dong, R. Maric, S. Pothukuchi, A. Hunt, Y. Li, and C.P. Wong, *J. Electron. Mater.* 34, 168 (2005).
5. E. Ide, S. Angata, A. Hirose, and K.F. Kobayashi, *Acta Mater.* 53, 2385 (2005).
6. T. Wang, X. Chen, G.Q. Lu, and G.Y. Lei, *J. Electron. Mater.* 36, 1333 (2007).
7. M. Maruyama, R. Matsubayashi, H. Iwakuro, S. Isoda, and T. Komatsu, *Appl. Phys. A* 93, 467 (2008).
8. S.J. Zhao, S.Q. Wang, D.Y. Cheng, and H.Q. Ye, *J. Phys. Chem. B* 105, 12857 (2001).
9. A.J. Gellman and Q. Dai, *J. Am. Chem. Soc.* 115, 714 (1993).
10. T. Mutsudome, Y. Mikami, H. Funai, T. Mizugaki, K. Jitsukawa, and K. Kaneda, *Angew. Chem. Int. Ed.* 47, 138 (2008).
11. A. Michota and J. Bukowska, *J. Raman Spectrosc.* 34, 21 (2003).
12. J.M. Anderson and J.K. Kochi, *J. Am. Chem. Soc.* 92, 1651 (1970).
13. H. Nagasawa, M. Maruyama, T. Komatsu, S. Isoda, and T. Kobayashi, *Phys. Stat. Sol. A* 191, 67 (2002).